



Cite this: *Phys. Chem. Chem. Phys.*,  
2017, 19, 30740

## Vibrational states of nano-confined water molecules in beryl investigated by first-principles calculations and optical experiments†

M. A. Belyanchikov,<sup>a</sup> E. S. Zhukova,<sup>a</sup> S. Tretiak,<sup>c,d</sup> A. Zhugayevych,<sup>d</sup> M. Dressel,<sup>ab</sup> F. Uhlig,<sup>d</sup> J. Smiatek,<sup>d</sup> M. Fyta,<sup>d</sup> V. G. Thomas<sup>d,f,g</sup> and B. P. Gorshunov<sup>ab</sup>

Using quantum mechanical calculations within density functional theory, we provide a comprehensive analysis of infrared-active excitation of water molecules confined in nanocages of a beryl crystal lattice. We calculate infrared-active modes including the translational, librational, and mixed-type resonances of regular and heavy water molecules. The results are compared to the experimental spectra measured for the two principal polarizations of the electric field: parallel and perpendicular to the crystallographic *c*-axis. Good agreement is achieved between calculated and measured isotopic shifts of the normal modes. We analyze the vibrational modes in connection with the structural characteristics and arrangements of water molecules within the beryl crystal. Specific atomic displacements are assigned to each experimentally detected vibrational mode resolving the properties of nano-confined water on scales not accessible by experiments. Our results elucidate the applicability and efficiency of a combined experimental and computational approach for describing and an in-depth understanding of nano-confined water, and pave the way for future studies of more complex systems.

Received 21st September 2017,  
Accepted 30th October 2017

DOI: 10.1039/c7cp06472a

rsc.li/pccp

### Introduction

High technological and fundamental interest towards water molecules confined in the cavities of nanometer size has stimulated numerous studies.<sup>1–9</sup> Knowledge of the properties of nano-confined water is important in geology, mineralogy, meteorology, chemistry and ionic liquids (*e.g.* ref. 10 and 11 and references therein). Specifically, hydration water poses a particular case, as it controls the structure, stability, functionality and reactivity of biomolecules.<sup>12–14</sup> Water is omnipresent at the boundaries of biological complexes and molecules as a hydration shell, for instance, in membrane channels and solutions, participating in hydrophobic/hydrophilic interactions, replication, and transcription processes.<sup>13</sup> On the other hand,

water at the nanoscale acquires qualitatively new properties, which are not observed in the bulk phase and are typically dictated by quantum mechanics and confined geometries (see, *e.g.* ref. 15). Understanding such systems is of great fundamental importance in the general context of revealing and ultimately controlling the mechanisms for the formation of new states of matter that emerge at the nanoscale and have potential applications in electronics.

Due to a labile and highly directional hydrogen bonding network, a relatively small moment of inertia and large dipole moment of the H<sub>2</sub>O molecule, bulk water remains one of the least understood liquids.<sup>16–19</sup> It is not surprising that the realm of nano-confined water is even more diverse and intricate. Consequently, the interpretation of experimental data and the formulation of quantitative physical (chemical, biological) models turn out to be extremely challenging. In such a situation, studies of simple nano-confined systems provide the much needed reference frame for the investigation of more complex cases. For example, studies of properties and dynamics of water in inert matrices and helium droplets led to unique insights into intermolecular interactions and formation of small clusters.<sup>20,21</sup> Excellent alternative systems are crystals with a lattice that contains rigid voids of the size suitable for hosting a single yet almost free H<sub>2</sub>O molecule (see, *e.g.* ref. 22 and 23). The well-defined and perfectly ordered geometry of the network of pores

<sup>a</sup> Moscow Institute of Physics and Technology, Dolgoprudny, Moscow Region, 141700, Russia. E-mail: belyanchikov@phystech.edu

<sup>b</sup> 1. Physikalisches Institut, Universität Stuttgart, 70569 Stuttgart, Germany

<sup>c</sup> Center for Integrated Nanotechnologies (CINT), Los Alamos National Laboratory, Los Alamos, NM 87545, USA

<sup>d</sup> Skolkovo Institute of Science and Technology, Moscow 143026, Russia

<sup>e</sup> Institute for Computational Physics, Universität Stuttgart, 70569 Stuttgart, Germany

<sup>f</sup> Sobolev Institute of Geology and Mineralogy, RAS, 630090 Novosibirsk, Russia

<sup>g</sup> Novosibirsk State University, Novosibirsk 630090, Russia

† Electronic supplementary information (ESI) available. See DOI: 10.1039/c7cp06472a

greatly simplifies experimental control and theoretical description of both single-molecule and collective properties of the water molecular subsystem.

One popular member of such crystal family is hydrous beryl. With the chemical composition  $\text{Be}_3\text{Al}_2\text{Si}_6\text{O}_{18}$ , beryl crystallizes in a honeycomb structure with the space group  $P6/mcc$ , consisting of stacked six-membered rings of  $\text{SiO}_4$  tetrahedra as depicted in Fig. 1. The latter leave relatively large open channels oriented parallel to the crystallographic  $c$ -axis.<sup>24,25</sup> Along this axis, the channels contain “bottlenecks” of approximately 2.8 Å alternating with slightly larger cages of 5.1 Å in diameter that can potentially host single  $\text{H}_2\text{O}$  molecules.<sup>26</sup> The  $\text{H}_2\text{O}$  molecules in beryl are held in two distinct orientations relative to the  $c$ -axis as displayed in Fig. 2. Type I and type II water molecules have the vector connecting two protons directed perpendicular and parallel to the  $c$ -axis, respectively.<sup>27</sup> Type II  $\text{H}_2\text{O}$  molecules are only found in crystals containing alkali ions ( $\text{Na}^+$ ,  $\text{Li}^+$ ) at the bottlenecks and interacting with the oxygen atom. Their dipole moments are turned by 90 degrees relative to the moments of water-I due to the Coulomb interaction of the water molecular oxygen with the alkaline cation in the neighboring pore. In all other cases the dipoles are oriented perpendicular to the  $c$ -axis; the molecular plane  $\text{H}-\text{O}-\text{H}$  is perpendicular to the  $ab$ -plane.

For such nano-confined systems, vibrational spectroscopy yields valuable information on how water couples to its cavity and on the interactions among the  $\text{H}_2\text{O}$  molecules in neighboring cages. This can be the basis for the development and synthesis of other cages of different geometries, and for deliberate doping in order to obtain targeted properties. Using broadband optical spectroscopy we have previously performed systematic and detailed experimental studies of the vibrational states of

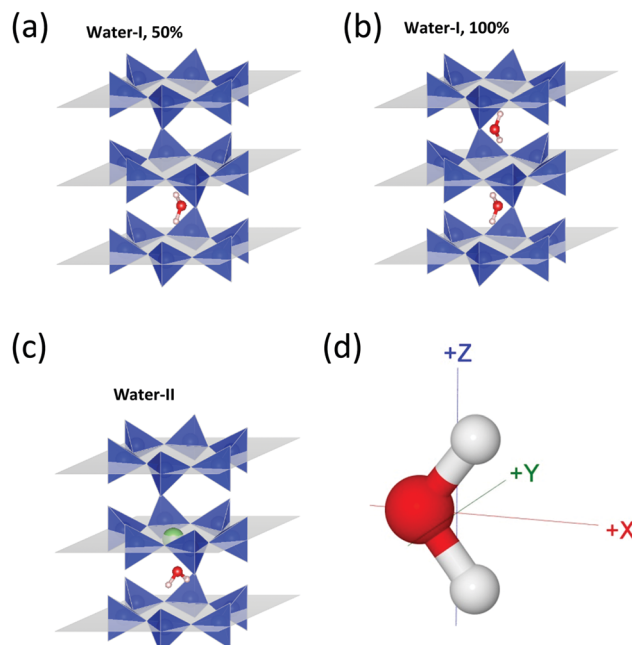


Fig. 2 Unit cells of beryl crystals with different fillings of the nanopores with water molecules considered in the present study: one water molecule of type I at (a) 50% and (b) 100% filling, respectively, and (c) one water molecule of type II with the alkali ion. (d) Orientation of the coordinate system used in notations of a free water molecule motion.

type I water molecules in crystalline beryl.<sup>28,29</sup> We discovered a rich and highly anisotropic set of absorption resonances occurring exclusively within the water molecular subsystem. When crystals contain alkali ions, additional modes appear due

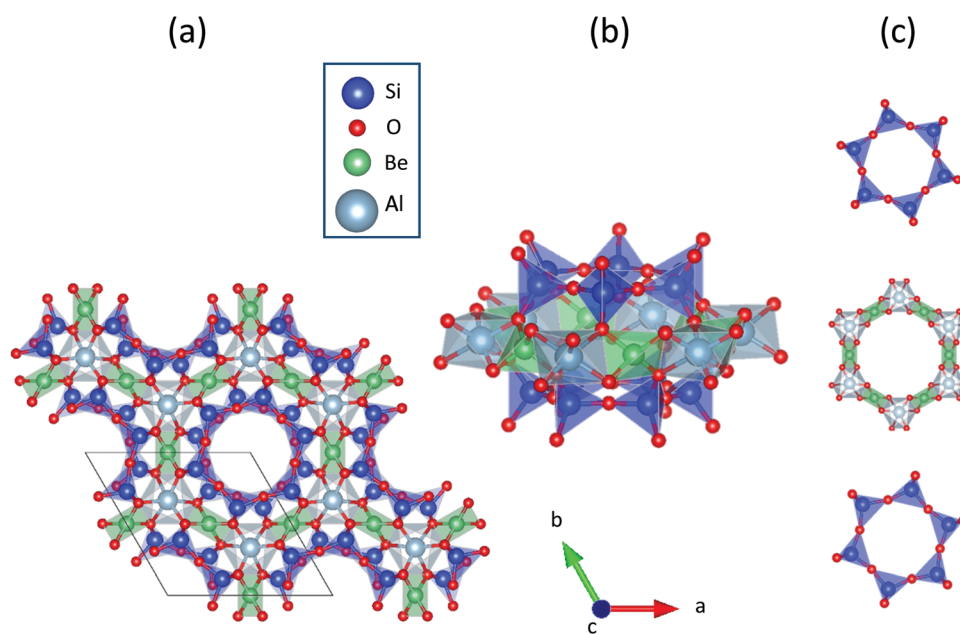
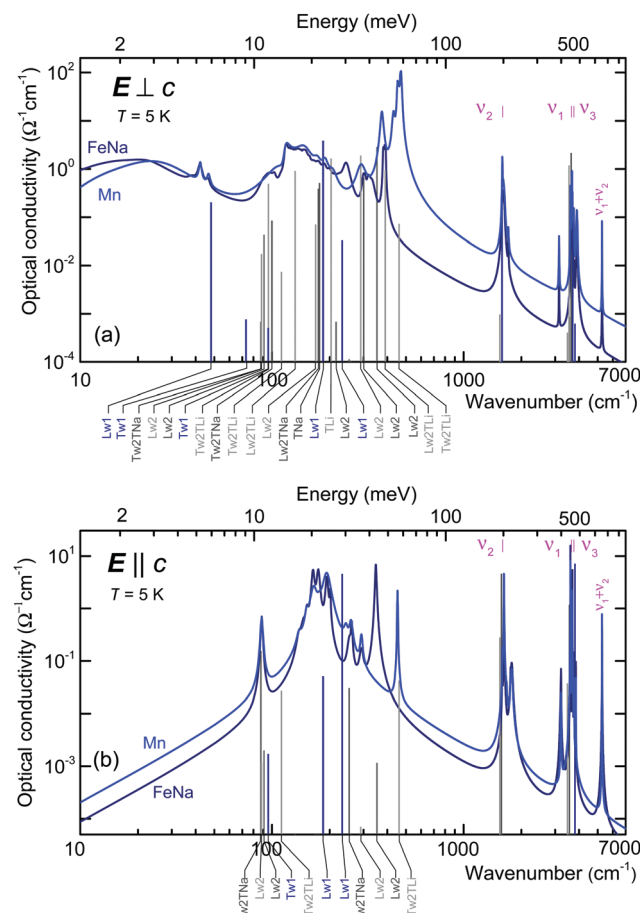


Fig. 1 Structure of the beryl crystal ( $\text{Be}_3\text{Al}_2\text{Si}_6\text{O}_{18}$ ). (a) The channels in the crystal lattice form a honeycomb structure (space group  $P6/mcc$ ). The crystallographic  $c$ -axis is perpendicular to the shown slice. (b) The channels consist of pores composed out of stacked silicon and aluminum rings separated by slightly narrower bottlenecks as depicted in (c). The color coding of the atoms is given in the legend.



**Fig. 3** Optical conductivity spectra of H<sub>2</sub>O molecules localized in beryllium crystalline nanopores. The spectra for two polarizations and for two different crystals are presented: "Mn" (blue color line) and "FeNa" (navy blue color line). The vertical bar denotes the calculated positions and intensities of the modes. To specify the types of modes, the following notations are used: L – librational; T – translational, w1 – water type I, w2 – water type II, Li – lithium, Na – sodium. For example, "Lw2TNa" means vibration involving librational motion of type II water molecule along with translational motion of the sodium ion. The cases of modes labeled Lw2 (Lw2TL, Lw2TNa) correspond to H<sub>2</sub>O libration around the c (*a*, *b*) axes. TLi and TNa correspond to translational modes of alkali ions with corresponding H<sub>2</sub>O translations negligibly small. Royal colored bars correspond to water type I at 50% filling, light gray and dark gray bars represent water type II calculated spectra with lithium and sodium, respectively.  $\nu_1$ ,  $\nu_2$  and  $\nu_3$  denote internal molecular modes.<sup>46</sup>

to the presence of type II water; the corresponding spectra are shown in Fig. 3. We have preliminarily assigned infrared (IR) resonances to translational and librational motions of the individual H<sub>2</sub>O molecules, which can tunnel between the neighboring minima of the crystalline six-well potential as proven by inelastic neutron scattering experiments.<sup>30</sup> The intramolecular H<sub>2</sub>O vibrational modes appear as additional peaks. The pronounced soft-mode behavior present at terahertz (THz) frequencies and below is associated with the emergence of an incipient ferroelectric phase due to interacting dipole moments of water molecules.<sup>31</sup> However, a theoretical interpretation of the relevant vibrational motions is still lacking. This motivates the present study to perform a comprehensive analysis of the IR-active single-particle vibrational states of

water molecules, including deuterated species, contained within the nanocages of the beryl crystal lattice. Our work combines broadband optical measurements and first-principles calculations within the density-functional-theory (DFT) approach. The results provide the foundation for future computational studies of similar systems.

## Experimental methodology

Vibrational states of nano-confined water are influenced by many factors. Here, we focus on the mass of the water molecules ( $\text{H}_2\text{O}$ ,  $\text{HDO}$ , and  $\text{D}_2\text{O}$ ) and the different amounts of alkali ions. Our experimental observations serve as a benchmark for theoretical modeling. We consider here our previous spectral data obtained for type I  $\text{H}_2\text{O}$  molecules<sup>28,29,31</sup> and complement them with new results obtained for beryl crystals containing heavy water molecules. In addition, measurements of beryl crystals containing alkali-ions were performed in order to observe vibrations of water type II molecules. All single crystals were grown in stainless steel autoclaves according to the standard hydrothermal growth method at a temperature of 600 °C and under a pressure of 1.5 kbar by recrystallization of natural beryl to a seed crystal.<sup>32</sup> The chemical analysis of the studied crystals is presented in Table S1 in the (ESI†). A standard Fourier transform spectrometer (Bruker Vertex 80v) was used to measure the spectra of reflection and transmission coefficients at frequencies from approximately 20  $\text{cm}^{-1}$  up to 7000  $\text{cm}^{-1}$  with 2  $\text{cm}^{-1}$  resolution. At sub-THz and THz frequencies, spectra of the complex dielectric permittivity and optical conductivity were directly determined using a quasioptical spectrometer based on monochromatic and continuously frequency tunable radiation generators – backward-wave oscillators<sup>33</sup> and a pulsed THz time-domain TeraView TPS Spectra 3000 spectrometer with 0.5  $\text{cm}^{-1}$  resolution. Water-related features in the spectra were verified by performing the same optical experiments on dehydrated samples obtained by heating the crystals up to 1000 °C and keeping under a vacuum for a period of about 24 hours. The comparative analysis of the spectra of samples with and without water allowed us to unambiguously distinguish water-related absorption resonances from those connected with phonons or impurities.<sup>29</sup>

## Computational methodology

First-principles DFT calculations were performed in the Vienna *Ab initio* Simulation Package (VASP).<sup>34–36</sup> For the basis-set and the exchange–correlation functional, the projector-augmented waves (PAW)<sup>37,38</sup> and the generalized gradient approximation (GGA) in the framework of Perdew–Burke–Ernzerhof (PBE)<sup>39</sup> were used. The van der Waals contributions to the interaction of water molecules with the cavity walls<sup>27</sup> were studied with PBE and the many-body dispersion energy corrections (here referred as PBE-MBD).<sup>40</sup> The energy cutoff for the plane wave basis set was fixed at 500 eV. The  $k$ -point sampling within the Brillouin zone was treated with the Monkhorst–Pack scheme using a

Gamma-centered  $5 \times 5 \times 5$   $k$ -mesh.<sup>41</sup> Gaussian smearing with 0.05 eV width was applied for orbital population in the energy minimization and force constant evaluation, whereas the tetrahedron method with Blöchl corrections was employed for single point calculations of the energy and density of states. The initial geometry of the crystal was taken from previous experimental work.<sup>42</sup> The beryl crystal was modeled by replication of the unit cell of beryl ( $\text{Al}_2\text{Be}_3\text{Si}_6\text{O}_{18}$ , two formula units per unit cell, 58 atoms in total) using periodic boundary conditions. One unit cell of beryl forms two pores, which can be filled with water molecules. In the present work, three possible filling options were considered to partially reproduce the actual conditions of the water molecules in the lattice (Fig. 2). The first two cases [Fig. 2(a) and (b)] with one and two water molecules in a unit cell correspond to a beryl crystal with 50 and 100% filling, respectively. The third case [Fig. 2(c)] reproduces the situation when the crystal contains a Li or Na ion coupled to a water molecule. The geometry of each structure was optimized by the conjugate gradient scheme with tight optimization criteria, resulting in gradients not exceeding 20 meV Å<sup>-1</sup>. The obtained lattice parameters are overestimated compared to the experimentally observed values, as was reported previously.<sup>30</sup> Accordingly, for all calculations we fixed the lattice parameters to the experimentally observed values ( $a = b = 9.208$  Å,  $c = 9.188$  Å for the three lattice parameters).<sup>42</sup> For each geometry described above, the vibrational normal modes and effective charge tensors were calculated using density functional perturbation theory (DFPT).<sup>43</sup> The oscillator strengths for IR-activity are given by

$$f(\nu) = \sum_{\alpha} \left| \sum_{s\beta} Z_{\alpha\beta}^*(s) e_{\beta}(s|\nu) \right|^2, \quad (1)$$

where  $e_{\beta}(s|\nu)$  is the normalized vibrational eigenvector of the  $\nu$ th mode,  $\alpha$  and  $\beta$  indicate Cartesian polarizations,  $s$  enumerates atoms in the unit cell, and  $Z_{\alpha\beta}^*(s)$  is the effective-charge tensor of the  $s$ th atom.

## Results and discussion

### 1. Geometry of water molecules in beryl crystals

Structural optimization upon constrained beryl lattice parameters as specified above results in different final geometries for each case. In the case where no alkali ions are present in the bottleneck, the water molecular dipole moment has its vector

lying within the  $(ab)$ -plane (water type I). In the case of water-II, an ion next to the water molecule at the center of the pores orients the water molecule in a way that the dipole moment points along the  $c$ -direction. Both geometries obtained agree with previous findings.<sup>27</sup> In the case of water-I, the protons occupy site 24m with the H–O–H plane approximately parallel to the  $(ac)$ -plane. The oxygen atom is slightly offset from the channel axis and calculated shifts are 0.21 Å and 0.14 Å for 50% and 100% filling, respectively, which are close to the values reported in a recent DFT study.<sup>30</sup> The vector connecting two protons of a H<sub>2</sub>O molecule is tilted by an angle of 1.58° in the case of two H<sub>2</sub>O molecules in the unit cell. It is slightly larger than 0.93° in the case of one molecule in the unit cell due to interaction between neighboring water molecules. The obtained deflection angle is larger than the value of 0.49° reported in recent DFT calculations,<sup>44</sup> but still smaller than 4° found experimentally at  $T = 300$  K.<sup>45</sup> The energy is the lowest for antiparallel dipole moments of the neighboring water molecules in the unit cell. The H–O–H angle of 104.6° and the O–H distance of 0.973 Å confirm previous results.<sup>44</sup> Table S2 in the ESI,<sup>†</sup> summarizes a complete list of the structural parameters for all configurations considered.

No essential difference was found in the geometry, potential energy landscape and vibrational frequencies by comparing results for the exchange-correlation functionals with and without dispersion corrections. This indicates the absence of specific non-covalent interactions between the water molecule and the surrounding crystal atoms. Accordingly, the crystal cage can be considered as producing an almost structureless potential well for intercalated molecules similar to that in fullerene.<sup>23</sup> The modulation of such potential by the crystal field is very small: the calculated barrier for rotation of the water-I molecule around the  $c$ -axis is less than 1 meV. In contrast to previous estimates,<sup>30</sup> our results are consistent with the temperature dependence of the experimentally obtained absorption spectra.<sup>31</sup>

### 2. Vibrational spectra of water molecules under vacuum

In the second step, we calculated the vibrational excitation of a simple model: type I water molecules spatially arranged as in the position given by the beryl crystal but with the lattice ions absent. The properties of such an artificial system are expected to be close to those of water vapor, enabling the comparison of our numerical results with literature values. Indeed, the calculated frequencies of the intramolecular modes  $\nu_1$ ,  $\nu_2$ , and  $\nu_3$  (Table 1)

**Table 1** Calculated (Calc.) and experimental<sup>46–48</sup> (Exp.) frequencies of intramolecular modes  $\nu_1$ ,  $\nu_2$ , and  $\nu_3$  for regular and heavy water molecules. These are spatially arranged under vacuum in a way they would be located within the beryl lattice, but with the lattice ions absent, as described in the text. Results are shown for the two water molecular filling factors, 50% and 100%. The numbers in the brackets indicate relative intensities for the two principal polarizations, parallel (||) and perpendicular (⊥) to the crystallographic  $c$ -axis

Mode type	H <sub>2</sub> O			D <sub>2</sub> O			HDO		
	Calc. (cm <sup>-1</sup> )		Exp.	Calc. (cm <sup>-1</sup> )		Exp.	Calc. (cm <sup>-1</sup> )		Exp.
	50%	100%		50%	100%		50%	100%	
$\nu_3$	3840.4 <sup>(   0.66)</sup>	3833.9 <sup>(   0.61)</sup>	3755.9	2812.1 <sup>(   0.78)</sup>	2807.2 <sup>(   0.72)</sup>	2787.7	3787.4 <sup>(   0.54)</sup>	3781.7 <sup>(   0.50)</sup>	3707.5
$\nu_1$	3730.3 <sup>(   0.01)</sup>	3738.0 <sup>(   0.01)</sup>	3657.1	2686.7 <sup>(   0.02)</sup>	2693.6 <sup>(   0.02)</sup>	2671.6	2747.6 <sup>(   0.23)</sup>	2743.3 <sup>(   0.21)</sup>	2723.7
$\nu_2$	1588.0 <sup>(   0.48)</sup>	1602.3 <sup>(   0.34)</sup>	1594.7	1161.9 <sup>(   0.47)</sup>	1172.0 <sup>(   0.32)</sup>	1178.4	1391.8 <sup>(   0.45)</sup>	1405.1 <sup>(   0.34)</sup>	1403.5

are in very good agreement (within 2.5%) with the relevant experimental results providing an important benchmark for the DFT models used in the present study.

In the beryl lattice, the inter-cavity distances are 4.6 Å and 9.2 Å, as viewed parallel and perpendicular to the *c*-axis, respectively. As a consequence, no hydrogen bonds exist between the water molecules as the effective interaction range is only 1–2 Å. The absence of hydrogen-bonds makes it possible to compare water molecules in beryl with a system of non-hydrogen bonded water species in pure liquid water.<sup>49</sup> Both systems have frequencies of intramolecular modes close to those in the gas phase. Despite the absence of hydrogen bonding, however, these molecules couple *via* the dipole–dipole mechanism since it has an effective interaction range of the order of 10–100 Å. With a molecular dipole moment of  $p = 1.85 \text{ D}^{50}$  we estimate a coupling energy of  $p^2/r^3 = 22 \text{ meV}$  and 2.8 meV, for the directions along and perpendicular to the *c*-axis, respectively. Our DFT calculations provide very close values of 24.2 meV and 2.1 meV, accounting for the fact that the water molecules are not point-dipoles.

### 3. Vibrational spectra of water molecules in beryl

We next focus on the vibrations of water molecules in the beryl crystal cage. The motion of these water molecules is restricted in all directions. Consequently, three translational modes  $T_{x,y,z}$  and three rotational modes  $R_{x,y,z}$  of a free molecule (Fig. 2(d)) transform into vibrations. In what follows, we refer to the restricted rotation-like modes as to librations. Their frequencies and identification are listed in Table 2. Patterns of free molecule motion modes preserve their identity and do not intermix for the water-I molecule in beryl; the only exception is found for the  $R_z$  and  $T_y$  modes. This mixing is related to the strong deviation of the potential energy surface in the *xy*-plane from a quadratic well. The depth of the pinning potential for the rotation of water-I molecules around the pore axis (crystallographic *c*-axis) is less than few meV. This means that water-I molecules are free to rotate

**Table 2** Calculated normal modes (at the  $\Gamma$ -point) of water molecules localized within nanopores of the beryl crystal lattice for 50% filling. Two types of calculations are shown: with beryl crystal lattice ions released and frozen according to optimized geometry. The modes are projected onto the motion of a free water molecule (3 translations  $T_{x,y,z}$ , 3 rotations  $R_{x,y,z}$ , 3 vibrations) oriented as in Fig. 2(d). The numbers in front of the type of motion indicate squared coefficients of the projection given as a percentage. The projection coefficients are shown only for motions that contribute to the normal mode more than 5%

Mode type	All atoms released		Lattice atoms frozen	
	$\nu, \text{cm}^{-1}$	Projection	$\nu, \text{cm}^{-1}$	Projection
$L_{z1}$	32 <sup>(±0.53)</sup> [0.00]	70 $T_y + 21R_z$	48 <sup>(±0.05)</sup> [0.00]	94 $T_y + 6R_z$
$T_x$	71 <sup>(±0.00)</sup> [0.00]	95 $T_x$	73 <sup>(±0.00)</sup> [0.00]	$T_x$
$T_z$	90 <sup>(±0.06)</sup> [0.01]	88 $T_z$	96 <sup>(±0.00)</sup> [0.01]	$T_z$
$L_{z2}$	109 <sup>(±1.00)</sup> [0.00]	16 $R_z + 17T_y$	185 <sup>(±1.00)</sup> [0.01]	92 $R_z + 5T_y$
$L_y$	222 <sup>(±0.34)</sup> [0.00]	51 $R_y$	232 <sup>(±0.64)</sup> [0.00]	98 $R_y$
$L_x$	228 <sup>(±0.00)</sup> [0.54]	42 $R_x$	257 <sup>(±0.00)</sup> [0.00]	$R_x$
$\nu_2$	1587 <sup>(±0.54)</sup> [0.00]	Bending	1586 <sup>(±0.32)</sup> [0.00]	Bending
$\nu_1$	3701 <sup>(±0.14)</sup> [0.00]	Sym. stretch	3703 <sup>(±0.09)</sup> [0.00]	Sym. stretch
$\nu_3$	3805 <sup>(±0.00)</sup> [1.00]	Asym. stretch	3808 <sup>(±0.00)</sup> [1.00]	Asym. stretch

around this axis at elevated temperature, whereas rotation in other directions is ceased. Subsequently, a water-I molecule can be viewed as a quasi-free rotator around the cage *c*-axis, since the lowest rotational excitations (a few meV in a fullerene cage<sup>23</sup>) are higher than the pinning potential, which is below 1 meV. Due to the misalignment between the cage axis and the molecular rotational axis, and since there is no strict cylindrical symmetry, the rotation strongly couples to other motions. This picture is fully confirmed by our adiabatic molecular dynamics analysis showing a complicated three-dimensional motion superimposed onto the two-dimensional rotation of the water molecule on the time-scale of a picosecond at room temperature. A more accurate modeling of this complex motion is beyond the scope of this work. Here, we rather focus on the vibrational IR-active modes in harmonic approximation. In order to simplify the calculation of IR intensities, we freeze the beryl lattice since the vibrational modes retain their identity to some extent even though being mixed with lattice modes (see Table 2). Table 3 summarizes the frequencies and relative intensities of all possible IR-active vibrations of water-I molecules ( $\text{H}_2\text{O}$ ,  $\text{D}_2\text{O}$ , DHO). For each type of crystal filling, three intramolecular, three librational and one translational modes are present. The other normal modes are IR-inactive and will not be considered in the further analysis.

Fig. 3 compares the calculated data with the experimental spectra containing resonances related exclusively to water vibrations with phonon absorption excluded.<sup>28,29,31</sup> Here and below, we discuss the experimental spectra of the optical conductivity (that is proportional to the absorption of the electromagnetic radiation) measured at liquid helium temperature for two principal polarizations: the electric field vector  $E$  parallel and perpendicular to the crystallographic *c*-axis. Experimental spectra of the two samples are very similar, certain differences in some line positions should be attributed to different impurities and water contents. The vertical bars in Fig. 3 display the excitations from our DFT modeling, with their heights corresponding to the relative intensity. As can be seen, the rich and anisotropic structures of experimental resonances are perfectly reproduced by calculated librational and translational vibrations of water-I and water-II molecules.

The DFT analysis allows us to identify types of ionic motions responsible for the observed modes, as indicated in Fig. 3 and explained in the caption and in Table S4 of the ESI.† For example, for the polarization  $E||c$ , the DFT calculations reveal two IR modes at  $184 \text{ cm}^{-1}$  ( $L_{z2}$ ) and at  $95 \text{ cm}^{-1}$  ( $T_z$ ) which are assigned to water-I librations and translations, respectively. The  $L_{z2}$  mode corresponds to the oscillation of the dipole moment in the plane that is parallel to the *c*-axis and the  $T_z$  mode corresponds to the motion of the entire water molecule along the *c*-axis (Fig. 2(d)). A translation mode of the same frequency was detected by neutron scattering.<sup>30</sup> For the perpendicular direction ( $E \perp c$ ) the far-IR absorption around  $100\text{--}500 \text{ cm}^{-1}$  is dominated by modes corresponding to the librations of mainly water-II molecules (labeled with  $L_{w2}\dots$ ) connected with noticeable concentration of alkali ions (Li, Na) present in the crystal (see Table S1, ESI†). The band also contains modes from vibrations of alkali ions

**Table 3** Calculated (Calc.) frequencies of normal modes for regular and heavy water molecules of type I in nanopores of the beryl crystal lattice.  $\nu_1$ ,  $\nu_2$  and  $\nu_3$  denote the internal molecular modes. L and T stand for librational and translational motions, respectively. The numbers in the brackets indicate relative intensities for the two principal polarizations, parallel (||) and perpendicular ( $\perp$ ) to the crystallographic *c*-axis

Mode type	$H_2O$		$D_2O$		$HDO$	
	Calc. ( $cm^{-1}$ )		Calc. ( $cm^{-1}$ )		Calc. ( $cm^{-1}$ )	
50%	100%		50%	100%	50%	100%
$\nu_3$	3807.9( $\perp 0.00$ ) ( $\parallel 1.00$ )	3801.5( $\perp 0.00$ ) ( $\parallel 1.00$ )	2789.3( $\perp 0.00$ ) ( $\parallel 1.00$ )	2784.0( $\perp 0.00$ ) ( $\parallel 1.00$ )	3757.5( $\perp 0.08$ ) ( $\parallel 1.00$ )	3753.4( $\perp 1.00$ ) ( $\parallel 1.00$ )
$\nu_1$	3703.3( $\perp 0.09$ ) ( $\parallel 0.00$ )	3703.0( $\perp 0.12$ ) ( $\parallel 0.00$ )	2667.0( $\perp 0.10$ ) ( $\parallel 0.00$ )	2668.0( $\perp 0.13$ ) ( $\parallel 0.00$ )	2726.3( $\perp 0.43$ ) ( $\parallel 0.43$ )	2723.7( $\perp 0.43$ ) ( $\parallel 0.43$ )
$\nu_2$	1585.6( $\perp 0.32$ ) ( $\parallel 0.00$ )	1585.3( $\perp 0.34$ ) ( $\parallel 0.00$ )	1160.0( $\perp 0.00$ ) ( $\parallel 0.31$ )	1159.5( $\perp 0.00$ ) ( $\parallel 0.32$ )	1391.1( $\perp 0.09$ ) ( $\parallel 0.45$ )	1391.5( $\perp 0.35$ ) ( $\parallel 0.35$ )
$L_y$	232.5( $\perp 0.01$ ) ( $\parallel 0.64$ )	196.3( $\perp 0.10$ ) ( $\parallel 0.56$ )	168.0( $\perp 0.01$ ) ( $\parallel 0.57$ )	143.0( $\perp 0.11$ ) ( $\parallel 0.49$ )	192.7( $\perp 0.00$ ) ( $\parallel 0.80$ )	165.1( $\perp 0.02$ ) ( $\parallel 0.73$ )
$L_{z2}$	184.8( $\perp 1.00$ ) ( $\parallel 0.01$ )	228.9( $\perp 1.00$ ) ( $\parallel 0.04$ )	131.4( $\perp 1.00$ ) ( $\parallel 0.01$ )	164.8( $\perp 1.00$ ) ( $\parallel 0.04$ )	144.5( $\perp 1.00$ ) ( $\parallel 0.01$ )	210.7( $\perp 1.00$ ) ( $\parallel 0.01$ )
$T_z$	95.7( $\perp 0.00$ ) ( $\parallel 0.01$ )	96.9( $\perp 0.00$ ) ( $\parallel 0.01$ )	90.4( $\perp 0.00$ ) ( $\parallel 0.01$ )	90.8( $\perp 0.00$ ) ( $\parallel 0.01$ )	93.0( $\perp 0.00$ ) ( $\parallel 0.01$ )	93.9( $\perp 0.00$ ) ( $\parallel 0.01$ )
$L_{z1}$	48.1( $\perp 0.05$ ) ( $\parallel 0.00$ )	56.4( $\perp 0.02$ ) ( $\parallel 0.00$ )	47.9( $\perp 0.09$ ) ( $\parallel 0.00$ )	55.4( $\perp 0.03$ ) ( $\parallel 0.00$ )	48.0( $\perp 0.09$ ) ( $\parallel 0.00$ )	55.9( $\perp 0.02$ ) ( $\parallel 0.00$ )

labeled with TLi and TNa. Lower-frequency translational modes ( $Tw_1, Tw_2\dots$ ) are located at or below  $100\text{ cm}^{-1}$ . One librational mode,  $Lw_1$ , is located at a very low frequency, at  $\approx 50\text{ cm}^{-1}$  for it corresponds to librations around the *c*-axis of a heavy oxygen ion. For both polarizations intramolecular modes  $\nu_1$ ,  $\nu_2$  and  $\nu_3$  are seen accompanied by the  $\nu_1 + \nu_2$  overtones at about  $5000\text{ cm}^{-1}$  and with their combinations with the lower-frequency excitation.<sup>28</sup>

An incomplete filling of the nanopores by  $H_2O$  molecules leads to an additional structure in the experimental spectra when water molecules are grouped into clusters of two and more molecules.<sup>31</sup> Molecular clustering should cause a certain renormalization of the excitation spectra due to interactions among the molecules in the cluster and between the molecules and the surrounding ions of the crystal lattice. This is confirmed by the analysis summarized in Table 3, where the frequencies of all vibrations are noticeably different for different filling factors. In particular, we are confident that two to four narrow peaks (Fig. 3 in the present paper and Fig. 3 in ref. 31) observed around  $40\text{--}50\text{ cm}^{-1}$  for  $E \perp c$  are related to librations of single water-I molecules and of these molecules within clusters of two and higher number of molecules. The compositions of the clusters and the corresponding spectral peaks intensities can be estimated within the combinatorial approach.<sup>28</sup>

#### 4. Experimental and theoretical isotopic shifts

A comparison of the experimentally determined excitations spectra for heavy and light water molecules helps in identifying spectral features that undergo a frequency shift when  $H_2O$  is replaced by  $D_2O$  or  $HDO$ . Since such an isotopic shift is uniquely related to the type of dynamics of the atoms participating in the corresponding oscillation, it allows us to independently obtain the value of the isotopic shift using the normal vectors of the water molecule calculated within DFPT. Comparing the experimental and computed isotopic shifts provides a reliable benchmark for the classification of water normal modes in beryl. Fig. 4 displays the measured optical conductivity spectra of a sample containing heavy water together with the calculated mode structure and their classification. Good overall agreement is observed between the experiment and calculations. The measured spectra are richer (see also intramolecular modes) since they contain resonances coming from DHO type II molecules that are also present

in real crystals;<sup>51</sup> the DFT data for these resonances are not shown for clarity reasons. Compared to light water, all resonances are shifted to lower frequencies, as presented in more details in Fig. 5 for frequencies below  $300\text{ cm}^{-1}$ . In the case of  $E \perp c$ , a significant difference between the experimental spectra was found in the frequency region associated with the librations  $L_{z2}$ . We can identify this vibration as hydrogen libration around the axis passing through the oxygen atom along the *c*-axis. For this motion replacing all mobile atoms by the corresponding isotope counterparts leads to the isotopic shift

$$\frac{\nu_{L_{z2}}(H_2O)}{\nu_{L_{z2}}(D_2O)} = \frac{\sqrt{2M_D}}{\sqrt{2M_H}} = \sqrt{2} \approx 1.41,$$

where  $M_H$  and  $M_D$  are the masses of hydrogen and deuterium, respectively. The frequencies of the  $L_{z2}$  mode obtained from our DFT analysis for light and heavy water yield a ratio of 1.41. As can be seen from Fig. 5, this value is in perfect agreement with the change in the corresponding spectral feature in the experimental spectra. The low-frequency librational mode  $L_{z1}$  involves the motion of the oxygen atom around the hydrogen atoms. Since in this case the substituted hydrogen atoms remain almost motionless, the isotopic shift is essentially absent corroborating our experimental observations:

$$\frac{\nu_{L_{z1}}(H_2O)}{\nu_{L_{z1}}(D_2O)} = \frac{\sqrt{M_O}}{\sqrt{M_O}} = 1.$$

A comparison with the experimental spectra for light and heavy water in the range of the  $L_{z1}$  mode reveals no distinguishable changes related to the isotopic shift.

Additionally, for the  $E \parallel c$  polarization, we obtain good agreement between the calculated and experimentally observed isotopic shifts of librational and translational modes  $L_y$  and  $T_z$ , as depicted in Fig. 4(b) and 5(b). Here, mode  $L_y$  is associated with hydrogen libration around the axis passing through the oxygen atom perpendicular to the *c*-axis. The mode exhibits the same frequency shift as the  $L_{z2}$  mode and

$$\frac{\nu_{L_y}(H_2O)}{\nu_{L_y}(D_2O)} = \frac{232.5\text{ cm}^{-1}}{168.0\text{ cm}^{-1}} \approx 1.38.$$

The experimentally determined shift coincides with the values from our DFT analysis.

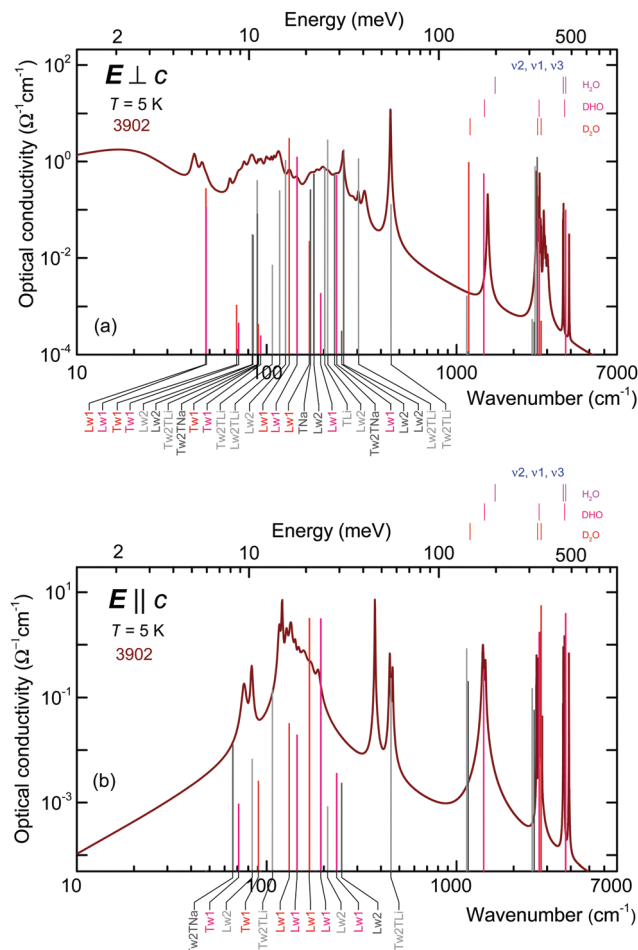


**Fig. 4** Optical conductivity spectra of  $\text{D}_2\text{O}$  and DHO molecules, localized in beryl crystalline nanopores. The spectra for two principal polarizations are presented: perpendicular (a) and parallel (b) to the crystallographic  $c$ -axis. The vertical bars show calculated positions and intensities of the modes. The red and pink bars correspond to  $\text{D}_2\text{O}$  and DHO water type I molecules at 50% filling, respectively. The light gray and dark gray bars represent the calculated spectra for type II  $\text{D}_2\text{O}$  water with lithium and sodium, respectively (water-II DHO modes are not presented to avoid the figure overload). The same notation as in Fig. 3 is used for specifying types of the modes.  $\nu_1$ ,  $\nu_2$  and  $\nu_3$  denote internal molecular modes for  $\text{H}_2\text{O}$ , HDO, and  $\text{D}_2\text{O}$  molecules.<sup>46–48</sup>

The translational mode  $T_z$  corresponds to translation of the whole  $\text{H}_2\text{O}$  molecule within the beryl cavity and is expected to have a minor isotopic shift according to

$$\frac{\nu_{T_z}(\text{H}_2\text{O})}{\nu_{T_z}(\text{D}_2\text{O})} = \frac{\sqrt{2M_{\text{D}} + M_{\text{O}}}}{\sqrt{2M_{\text{H}} + M_{\text{O}}}} = 1.05.$$

The same weak isotopic shift is found in the experimental spectra shown in Fig. 5.

We note that the intensities of light and heavy water resonances are almost the same at high frequencies above  $100 \text{ cm}^{-1}$ , Fig. 5. Interestingly, they differ significantly at lower frequencies that can be explained by a larger amplitude of atomic displacements and the corresponding stronger differences in localizing the potential felt by light and heavy water molecules. From the perfect agreement of the measured and

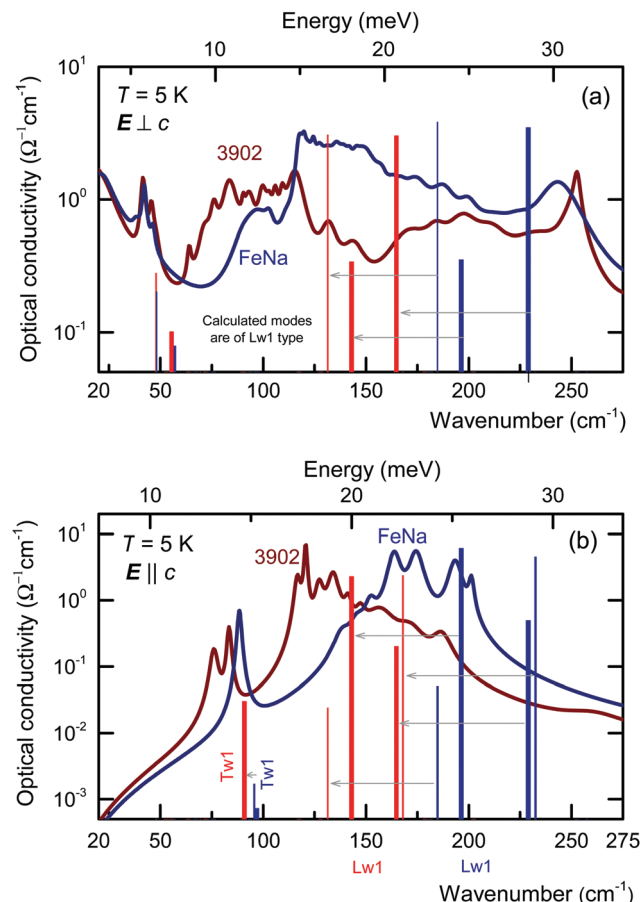


**Fig. 5** Far-infrared optical conductivity spectra of water molecules localized in beryl crystalline nanopores. The spectra for two polarizations and for two different crystals are presented: "FeNa" (navy color line) containing  $\text{H}_2\text{O}$  molecules and "3902" (wine color lines) containing  $\text{D}_2\text{O}$  and DHO molecules. Vertical bars show the calculated positions and intensities of the modes. Red and royal color bars represent calculated spectra for  $\text{H}_2\text{O}$  and  $\text{D}_2\text{O}$  molecules, respectively. Modes labeled Lw1 and Tw1 correspond to librational and translational modes of water type I molecules (data for water-II are not shown). Thin and thick bars represent 50% and 100% filling, respectively. Arrows show isotopic shifts. No shift is observed for the lines around  $50\text{--}60 \text{ cm}^{-1}$ ,  $E \perp c$ , since these are connected with oxygen motion.

calculated isotopic shifts, we conclude that the performed DFT analysis not only provides the correct frequency positions of the modes, but also determines correctly the character of specific atomic displacements within these modes.

## 5. Other structural features of the experimental spectra

We note that there exist additional structures in the measured THz spectra that are not considered in the above analysis. The complex band around  $10\text{--}40 \text{ cm}^{-1}$ , for instance, is connected to the ferroelectric soft mode that is a fingerprint of the emerging incipient ferroelectric state.<sup>31</sup> Due to the collective character of the band, it is not reproduced by the normal mode analysis of single water molecules considered here. In addition, for both polarizations the measured intramolecular modes  $\nu_1$ ,  $\nu_2$  and  $\nu_3$  are accompanied by combinational bands including the pronounced peaks for  $\text{H}_2\text{O}$ , HDO, and  $\text{D}_2\text{O}$  at  $\nu_1 + \nu_2$  and

combinations with lower-frequency modes. Additional lines in the experimental spectra originate from the splitting of the energy states of water molecules due to tunneling of protons in the six-well crystalline potential as confirmed by neutron scattering experiments.<sup>30</sup> Since our analysis is based on a harmonic approximation, the computed results cannot reproduce the excitation spectrum of the complex three-dimensional motion of a water molecule in a cage, including tunnel splitting between equivalent minima on the potential energy surface. Going beyond this approximation may allow us to identify and analyze this energy splitting, and other quantum and collective phenomena, which can be a subject of a separate study.

## Conclusions

We have performed first-principles calculations of the infrared-active excitation of light and heavy water molecules, H<sub>2</sub>O, D<sub>2</sub>O and DHO, confined to nanocages in the lattice of crystalline beryl. Equilibrium structures are obtained for several typical experimental configurations such as water molecules of type I at 50% and 100% filling, as well as type II water molecules with an alkali ion. Vibrational spectra (including vibration type, frequency, and IR intensity) were calculated and compared with measured experimental spectra on beryl crystals with light and heavy water molecules. Good agreement is found between calculated and observed values for all librational, translational and mixed-type vibrations arising from water molecules coupled to alkali ions. The investigation of the isotope shift of the IR resonances confirms the character of the atomic displacement in each mode.

We have demonstrated that DFT-modeling is suitable for the analysis of the nature of excitation of nano-confined water as well as other types of molecules and molecular complexes. Accordingly, DFT calculations can be used for further investigations of similar systems. Overall, this study paves the way for future work that will use electronic structure simulations of nano-confined molecular systems together with experimental results for an in-depth understanding of more complex dynamics such as collective (*e.g.*, incipient ferroelectric states) and quantum (*e.g.*, proton tunneling) phenomena pronounced in this unique class of materials. Our future studies will include additional quasi-1D crystals for elucidating the inherent characteristics of nano-confined water.

## Conflicts of interest

There are no conflicts to declare.

## Acknowledgements

The work was supported by the Russian Ministry of Education and Science (Program ‘5top100’), Project N3.9896.2017/BY and MIPT grant for visiting professors. F. U. J. S., and M. F. acknowledge financial support from collaborative network SFB 716 “Dynamic simulations of systems with large particle

numbers” funded by the German Funding Agency (Deutsche Forschungsgemeinschaft-DFG). The simulations of this work were performed on the computational resource ForHLR Phase I and the bwUniCluster funded by the Ministry of Science, Research and Arts Baden-Württemberg and the Universities of the State of Baden-Württemberg, Germany, within the framework program bwHPC. This work was conducted, in part, at the Center for Integrated Nanotechnologies, a U.S. Department of Energy, Office of Basic Energy Sciences user facility at Los Alamos National Laboratory (LANL). We thank G. Untereiner for sample preparation and K.N.Boldyrev for assistance with infrared experiments.

## References

- 1 G. F. Reiter, A. I. Kolesnikov, S. J. Paddison, P. M. Platzman, A. P. Moravsky, M. A. Adams and J. Mayers, *Phys. Rev. B: Condens. Matter Mater. Phys.*, 2012, **85**, 045403.
- 2 D. J. Mann and M. D. Halls, *Phys. Rev. Lett.*, 2003, **90**, 195503.
- 3 K. Koga, G. T. Gao, H. Tanaka and X. C. Zeng, *Nature*, 2001, **412**, 802–805.
- 4 A. I. Kolesnikov, J.-M. Zanotti, C.-K. Loong, P. Thiagarajan, A. P. Moravsky, R. O. Loutfy and C. J. Burnham, *Phys. Rev. Lett.*, 2004, **93**, 035503.
- 5 J. K. Holt, H. G. Park, Y. Wang, M. Stadermann, A. B. Artyukhin, C. P. Grigoropoulos, A. Noy and O. Bakajin, *Science*, 2006, **312**, 1034–1037.
- 6 Y. Maniwa, K. Matsuda, H. Kyakuno, S. Ogasawara, T. Hibi, H. Kadowaki, S. Suzuki, Y. Achiba and H. Kataura, *Nat. Mater.*, 2007, **6**, 135–141.
- 7 G. Hummer, J. C. Rasaiah and J. P. Noworyta, *Nature*, 2001, **414**, 188–190.
- 8 C. Dellago, M. M. Naor and G. Hummer, *Phys. Rev. Lett.*, 2003, **90**, 105902.
- 9 C. Dellago and G. Hummer, *Phys. Rev. Lett.*, 2006, **97**, 245901.
- 10 A. Nalaparaju, R. Babarao, X. S. Zhao and J. W. Jiang, *ACS Nano*, 2009, **3**, 2563–2572.
- 11 V. S. Gorelik and V. V. Filatov, *Bull. Lebedev Phys. Inst.*, 2012, **39**, 311–319.
- 12 R. Gregory, *Protein-Solvent Interactions*, CRC Press, New York, 1995.
- 13 G. W. Robinson, S. Singh, S. B. Zhu and M. W. Evans, *Water in Biology, Chemistry and Physics: Experimental Overviews and Computational Methodologies*, World Scientific, Singapore, 1996.
- 14 B. Hille, *Ionic Channels of Excitable Membranes*, Sinauer Associates, Sunderland, 2001.
- 15 T. Mizota, N. Satake, K. Fujiwara and N. Nakayama, Proceedings of the 13th International Conference on the Properties of Water and Steam, NRC Research Press, Ottawa, Canada, 2000.
- 16 F. Franks, *Water: A Matrix of Life*, 2nd ed, The Royal Society of Chemistry, Cambridge, 2000.
- 17 S. Solomon, *Water: The Epic Struggle for Wealth, Power, and Civilization*, Harper, New York, 2010.

- 18 M. Chaplin, in *Water The Forgotten Biological Molecule*, ed. D. LeBihan and H. Fukuyama, Pan Stanford Publishing, Singapore, 2010, vol. 1, pp. 3–19.
- 19 L. Pauling, *General Chemistry*, 3rd ed, Dover, New York, 1988.
- 20 K. Nauta and R. E. Miller, *Science*, 2000, **287**, 293–295.
- 21 R. E. Miller and S. S. Xantheas, *J. Am. Chem. Soc.*, 2017, **139**, 4152–4156.
- 22 B. A. Kolesov, *J. Struct. Chem.*, 2006, **47**, 21–34.
- 23 C. Beduz, M. Carravetta, J. Y.-C. Chen, M. Concistrè, M. Denning, M. Frunzi, A. J. Horsewill, O. G. Johannessen, R. Lawler, X. Lei, M. H. Levitt, Y. Li, S. Mamone, Y. Murata, U. Nagel, T. Nishida, J. Ollivier, S. Rols, T. Rööm, R. Sarkar, N. J. Turro and Y. Yang, *Proc. Natl. Acad. Sci.*, 2012, **109**, 12894–12898.
- 24 G. V. Gibbs, D. W. Breck and E. P. Meagher, *Lithos*, 1968, **1**, 275–285.
- 25 B. Morosin, *Acta Crystallogr., Sect. B: Struct. Crystallogr. Cryst. Chem.*, 1972, **28**, 1899–1903.
- 26 R. I. Mashkovtsev, E. S. Stoyanov and V. G. Thomas, *J. Struct. Chem.*, 2004, **45**, 56–63.
- 27 D. L. Wood and K. Nassau, *Am. Mineral.*, 1968, **53**, 777–800.
- 28 B. P. Gorshunov, E. S. Zhukova, V. I. Torgashev, V. V. Lebedev, G. S. Shakurov, R. K. Kremer, E. V. Pestrikov, V. G. Thomas, D. A. Fursenko and M. Dressel, *J. Phys. Chem. Lett.*, 2013, **4**, 2015–2020.
- 29 E. S. Zhukova, V. I. Torgashev, B. P. Gorshunov, V. V. Lebedev, G. S. Shakurov, R. K. Kremer, E. V. Pestrikov, V. G. Thomas, D. A. Fursenko, A. S. Prokhorov and M. Dressel, *J. Chem. Phys.*, 2014, **140**, 224317.
- 30 A. I. Kolesnikov, G. F. Reiter, N. Choudhury, T. R. Prisk, E. Mamontov, A. Podlesnyak, G. Ehlers, A. G. Seel, D. J. Wesolowski and L. M. Anovitz, *Phys. Rev. Lett.*, 2016, **116**, 167802.
- 31 B. P. Gorshunov, V. I. Torgashev, E. S. Zhukova, V. G. Thomas, M. A. Belyanchikov, C. Kadlec, F. Kadlec, M. Savinov, T. Ostapchuk, J. Petzelt, J. Prokleška, P. V. Tomas, E. V. Pestrikov, D. A. Fursenko, G. S. Shakurov, A. S. Prokhorov, V. S. Gorelik, L. S. Kadyrov, V. V. Uskov, R. K. Kremer and M. Dressel, *Nat. Commun.*, 2016, **7**, 12842.
- 32 V. G. Thomas and V. A. Klyakhin, *Mineral Forming in Endogenic Processes*, Nauka, Novosibirsk, USSR, 1987.
- 33 B. Gorshunov, A. Volkov, I. Spektor, A. Prokhorov, A. Mukhin, M. Dressel, S. Uchida and A. Loidl, *Int. J. Infrared Millimeter Waves*, 2005, **26**, 1217–1240.
- 34 G. Kresse and J. Hafner, *Phys. Rev. B: Condens. Matter Mater. Phys.*, 1994, **49**, 14251–14269.
- 35 G. Kresse and J. Furthmüller, *Comput. Mater. Sci.*, 1996, **6**, 15–50.
- 36 W. Kohn and L. J. Sham, *Phys. Rev.*, 1965, **140**, A1133–A1138.
- 37 P. E. Blöchl, *Phys. Rev. B: Condens. Matter Mater. Phys.*, 1994, **50**, 17953–17979.
- 38 G. Kresse and D. Joubert, *Phys. Rev. B: Condens. Matter Mater. Phys.*, 1999, **59**, 1758–1775.
- 39 J. P. Perdew, K. Burke and M. Ernzerhof, *Phys. Rev. Lett.*, 1996, **77**, 3865–3868.
- 40 A. Tkatchenko, R. A. DiStasio, R. Car and M. Scheffler, *Phys. Rev. Lett.*, 2012, **108**, 236402.
- 41 H. J. Monkhorst and J. D. Pack, *Phys. Rev. B: Condens. Matter Mater. Phys.*, 1976, **13**, 5188–5192.
- 42 R. M. Hazen, A. Y. Au and L. W. Finger, *Am. Mineral.*, 1986, **71**, 977–984.
- 43 S. Baroni, S. de Gironcoli, A. Dal Corso and P. Giannozzi, *Rev. Mod. Phys.*, 2001, **73**, 515–562.
- 44 Y. Finkelstein, R. Moreh, S. L. Shang, Y. Wang and Z. K. Liu, *J. Chem. Phys.*, 2017, **146**, 124307.
- 45 G. D. Gatta, F. Nestola, G. D. Bromiley and S. Mattauch, *Am. Mineral.*, 2006, **91**, 29–34.
- 46 J. Tennyson, P. F. Bernath, L. R. Brown, A. Campargue, A. G. Császár, L. Daumont, R. R. Gamache, J. T. Hodges, O. V. Naumenko, O. L. Polyansky, L. S. Rothman, A. C. Vandaele, N. F. Zobov, A. R. A. Derzi, C. Fábri, A. Z. Fazliev, T. Furtenbacher, I. E. Gordon, L. Lodi and I. I. Mizus, *J. Quant. Spectrosc. Radiat. Transfer*, 2013, **117**, 29–58.
- 47 J. Tennyson, P. F. Bernath, L. R. Brown, A. Campargue, A. G. Császár, L. Daumont, R. R. Gamache, J. T. Hodges, O. V. Naumenko, O. L. Polyansky, L. S. Rothman, R. A. Toth, A. C. Vandaele, N. F. Zobov, S. Fally, A. Z. Fazliev, T. Furtenbacher, I. E. Gordon, S.-M. Hu, S. N. Mikhailenko and B. A. Voronin, *J. Quant. Spectrosc. Radiat. Transfer*, 2010, **111**, 2160–2184.
- 48 J. Tennyson, P. F. Bernath, L. R. Brown, A. Campargue, A. G. Császár, L. Daumont, R. R. Gamache, J. T. Hodges, O. V. Naumenko, O. L. Polyansky, L. S. Rothman, A. C. Vandaele, N. F. Zobov, N. Dénes, A. Z. Fazliev, T. Furtenbacher, I. E. Gordon, S.-M. Hu, T. Szidarovszky and I. A. Vasilenko, *J. Quant. Spectrosc. Radiat. Transfer*, 2014, **142**, 93–108.
- 49 J. D. Eaves, J. J. Loparo, C. J. Fecko, S. T. Roberts, A. Tokmakoff and P. L. Geissler, *Proc. Natl. Acad. Sci. U. S. A.*, 2005, **102**, 13019–13022.
- 50 D. R. Linde, *CRC Handbook of Chemistry and Physics*, 80th ed, CRC Press, Boca Raton, Florida, 1999.
- 51 R. I. Mashkovtsev, V. G. Thomas, D. A. Fursenko, E. S. Zhukova, V. V. Uskov and B. P. Gorshunov, *Am. Mineral.*, 2016, **101**, 175–180.

**Supplementary Information For  
Vibrational states of nano-confined water molecules in beryl investigated by first principles  
calculations and optical experiments**

M.A.Belyanchikov<sup>1,2</sup>, E.S.Zhukova<sup>1</sup>, S.Tretiak<sup>3,4</sup>, A.Zhugayevych<sup>4</sup>, M. Dressel<sup>1,2</sup>, F. Uhlig<sup>5</sup>, J. Smiatek<sup>5</sup>, M. Fyta<sup>5</sup>, V.G.Thomas<sup>6,7</sup>, and B.P. Gorshunov<sup>1,2</sup>

<sup>1</sup>*Moscow Institute of Physics and Technology, Dolgoprudny, Moscow Region, 141700 Russia*

<sup>2</sup>*1. Physikalisches Institut, Universität Stuttgart, 70569 Stuttgart, Germany*

<sup>3</sup>*Center for Integrated Nanotechnologies (CINT), Los Alamos National Laboratory, Los Alamos, NM 87545, U.S.A.*

<sup>4</sup>*Skolkovo Institute of Science and Technology, Moscow 143026, Russia*

<sup>5</sup>*Institute for Computational Physics, Universität Stuttgart, 70569 Stuttgart, Germany*

<sup>6</sup>*Sobolev Institute of Geology and Mineralogy, RAS, 630090 Novosibirsk, Russia*

<sup>7</sup>*Novosibirsk State University, Novosibirsk 630090, Russia*

Table S1. Chemical composition (in wt. %) of the hydrous beryl crystals used for the measurements of terahertz-infrared excitation spectra of nanocaged water molecules.

Sample name (water molecule type)	SiO <sub>2</sub>	Al <sub>2</sub> O <sub>3</sub>	BeO	Fe <sub>2</sub> O <sub>3</sub>	MnO	Cr <sub>2</sub> O <sub>3</sub>	CuO	Li <sub>2</sub> O	Na <sub>2</sub> O	LOI*	Total
FeNa (H <sub>2</sub> O)	66.12	18.27	13.86	0.60	0.00	0.00	0.01	0.02	0.05	0.85	99.78
Mn (H <sub>2</sub> O)	66.79	17.32	13.75	1.30	0.09	0.00	0.00	0.15	0.00	1.93	101.18
3902 (D <sub>2</sub> O, DHO)	66.18	18.66	13.80	0.05	0.00	0.00	0.00	0.04	0.00	1.14	99.87

\*LOI: loss on ignition.

Table S2. Calculated geometries of water molecules in nanopores of beryl crystal lattice. The data for 50% and 100% fillings of crystalline pores are presented. Results corresponding to water molecules that are spatially arranged in vacuum in an arrangement as in the beryl lattice, but with the lattice ions absent (see text) are also given.

Water geometry	HOH angle (deg.)	OH distance (Å)	HH distance (Å)
Water type I in vacuum, 50% filling	104.39	0.972	1.536
Water type I in vacuum, 100% filling	104.33	0.972	1.536
Water vapor (exp. <sup>S1</sup> )	104.47	0.957	1.513
Water type I in beryl, 50% filling	105.07	0.973	1.545
Water type I in beryl, 100% filling	104.59	0.973	1.540
Water type II + Li in beryl	105.08	0.983	1.560
Water type II + Na in beryl	103.69	0.979	1.541

Table S3. Comparison of the vibrational frequencies (in cm<sup>-1</sup>) of the modes calculated by different methods. Here DFPT refers to density functional perturbation theory, and FD means finite differences, PBE - Perdew-Burke-Ernzerhof exchange-correlation functional,<sup>S2</sup> MBD - many-body dispersion energy correction.<sup>S3</sup> Negative values indicate imaginary frequencies.

Mode type	PBE/DFPT	PBE/FD	PBE-MBD/FD
L <sub>z1</sub>	32	-73	-50
T <sub>x</sub>	71	54	49
T <sub>z</sub>	90	78	86
L <sub>z2</sub>	109	107	92
L <sub>y</sub>	222	219	220
L <sub>x</sub>	228	230	222
bending	1587	1586	1580
sym. stretch	3701	3708	3702
asym. stretch	3805	3807	3805

Table S4. Normal modes and their frequencies (in  $\text{cm}^{-1}$ ) of complexes involving water-II molecules and alkali ions.  $v_1$ ,  $v_2$  and  $v_3$  denote internal  $\text{H}_2\text{O}$  molecular modes. L and T stand for librational and translational motions, respectively. The numbers in the brackets indicate relative intensities for two principle polarizations, parallel ( $\parallel$ ) and perpendicular ( $\perp$ ) to the crystallographic  $c$ -axis. The cases of modes labeled Lw2 (Lw2TLi, LwTNa) correspond to  $\text{H}_2\text{O}$  libration around c (a, b) axes. TLi, TNa correspond to translational modes of alkali ions with corresponding  $\text{H}_2\text{O}$  translations negligibly small.

<i>Li</i>				<i>Na</i>			
Mode type	$H_2O$	$D_2O$	$DHO$	Mode type	$H_2O$	$D_2O$	$DHO$
$v_3$	3540.4( $\pm 0.62$ ) ( $\parallel 0.00$ )	2591.4( $\pm 0.28$ ) ( $\parallel 0.00$ )	3508.9( $\pm 0.37$ ) ( $\parallel 0.10$ )	$v_3$	3634.0( $\pm 0.75$ ) ( $\parallel 0.00$ )	2659.5( $\pm 0.70$ ) ( $\parallel 0.00$ )	3599.1( $\pm 0.52$ ) ( $\parallel 0.15$ )
$v_1$	3475.4( $\pm 0.00$ ) ( $\parallel 0.13$ )	2505.0( $\pm 0.00$ ) ( $\parallel 0.18$ )	2547.0( $\pm 0.17$ ) ( $\parallel 0.06$ )	$v_1$	3562.7( $\pm 0.00$ ) ( $\parallel 0.26$ )	2567.8( $\pm 0.00$ ) ( $\parallel 0.29$ )	2613.1( $\pm 0.23$ ) ( $\parallel 0.10$ )
$v_2$	1544.3( $\pm 0.00$ ) ( $\parallel 1.00$ )	1132.3( $\pm 0.00$ ) ( $\parallel 1.00$ )	1357.7( $\pm 0.02$ ) ( $\parallel 1.00$ )	$v_2$	1575.0( $\pm 0.00$ ) ( $\parallel 1.00$ )	1152.8( $\pm 0.00$ ) ( $\parallel 1.00$ )	1382.8( $\pm 0.02$ ) ( $\parallel 1.00$ )
$Tw2TLi$	459.8( $\pm 0.04$ ) ( $\parallel 0.15$ )	451.9( $\pm 0.05$ ) ( $\parallel 0.28$ )	457.3( $\pm 0.05$ ) ( $\parallel 0.20$ )	$Lw2$	353.0( $\pm 1.00$ ) ( $\parallel 0.00$ )	254.5( $\pm 1.00$ ) ( $\parallel 0.00$ )	315.8( $\pm 1.00$ ) ( $\parallel 0.00$ )
$Lw2TLi$	390.3( $\pm 0.49$ ) ( $\parallel 0.00$ )	304.8( $\pm 0.41$ ) ( $\parallel 0.00$ )	337.1( $\pm 0.55$ ) ( $\parallel 0.00$ )	$Lw2$	300.7( $\pm 0.23$ ) ( $\parallel 0.00$ )	248.3( $\pm 0.00$ ) ( $\parallel 0.01$ )	264.6( $\pm 0.13$ ) ( $\parallel 0.00$ )
$Lw2$	290.4( $\pm 1.00$ ) ( $\parallel 0.00$ )	209.7( $\pm 1.00$ ) ( $\parallel 0.00$ )	256.8( $\pm 0.91$ ) ( $\parallel 0.00$ )	$Tw2TNa$	252.7( $\pm 0.00$ ) ( $\parallel 0.01$ )	228.1( $\pm 0.33$ ) ( $\parallel 0.00$ )	243.5( $\pm 0.12$ ) ( $\parallel 0.00$ )
$TLi$	203.4( $\pm 0.87$ ) ( $\parallel 0.00$ )	202.3( $\pm 0.26$ ) ( $\parallel 0.00$ )	203.8( $\pm 1.00$ ) ( $\parallel 0.00$ )	$Lw2$	215.9( $\pm 0.00$ ) ( $\parallel 0.00$ )	177.3( $\pm 0.32$ ) ( $\parallel 0.00$ )	177.5( $\pm 0.26$ ) ( $\parallel 0.00$ )
$Lw2$	168.9( $\pm 0.04$ ) ( $\parallel 0.00$ )	125.7( $\pm 0.38$ ) ( $\parallel 0.00$ )	136.0( $\pm 0.19$ ) ( $\parallel 0.00$ )	$TNa$	176.9( $\pm 0.18$ ) ( $\parallel 0.00$ )	170.1( $\pm 0.15$ ) ( $\parallel 0.00$ )	173.0( $\pm 0.14$ ) ( $\parallel 0.00$ )
$Lw2TLi$	132.1( $\pm 0.48$ ) ( $\parallel 0.00$ )	117.1( $\pm 0.09$ ) ( $\parallel 0.00$ )	127.0( $\pm 0.43$ ) ( $\parallel 0.00$ )	$Lw2TNa$	174.6( $\pm 0.14$ ) ( $\parallel 0.00$ )	152.6( $\pm 0.00$ ) ( $\parallel 0.00$ )	172.2( $\pm 0.01$ ) ( $\parallel 0.00$ )
$Tw2TLi$	111.9( $\pm 0.00$ ) ( $\parallel 0.10$ )	107.1( $\pm 0.00$ ) ( $\parallel 0.17$ )	108.3( $\pm 0.02$ ) ( $\parallel 0.12$ )	$Tw2TNa$	99.9( $\pm 0.03$ ) ( $\parallel 0.00$ )	89.3( $\pm 0.05$ ) ( $\parallel 0.00$ )	92.9( $\pm 0.04$ ) ( $\parallel 0.00$ )
$Tw2TLi$	95.8( $\pm 0.26$ ) ( $\parallel 0.00$ )	89.2( $\pm 0.14$ ) ( $\parallel 0.00$ )	90.9( $\pm 0.23$ ) ( $\parallel 0.00$ )	$Lw2$	90.9( $\pm 0.01$ ) ( $\parallel 0.00$ )	84.8( $\pm 0.02$ ) ( $\parallel 0.00$ )	86.3( $\pm 0.01$ ) ( $\parallel 0.00$ )
$Lw2$	88.2( $\pm 0.01$ ) ( $\parallel 0.00$ )	83.3( $\pm 0.01$ ) ( $\parallel 0.01$ )	83.3( $\pm 0.01$ ) ( $\parallel 0.00$ )	$Tw2TNa$	87.6( $\pm 0.00$ ) ( $\parallel 0.03$ )	66.4( $\pm 0.00$ ) ( $\parallel 0.06$ )	67.2( $\pm 0.00$ ) ( $\parallel 0.04$ )

## References

- S1 J. B. Hasted, in *The Physics and Physical Chemistry of Water*, ed. F. Franks, Springer, New York, 1972, 255-309.
- S2 J. P. Perdew, K. Burke and M. Ernzerhof, *Phys. Rev. Lett.*, 1996, **77**, 3865-3868.
- S3 A. Tkatchenko, R. A. DiStasio, R. Car and M. Scheffler, *Phys. Rev. Lett.*, 2012, **108**, 236402.